Journal of Marine Research, 57, 29–45, 1999

Modeling the Antarctic Circumpolar Current: A comparison of FRAM and equivalent barotropic model results

by V. O. Ivchenko[1,2], A. E. Krupitsky[3], V. M. Kamenkovich[4] and N. C. Wells[1]

ABSTRACT

Analyzing the FRAM simulations, Killworth (1992) noticed a strong tendency for self-similarity in the vertical structure of the velocity field of the Antarctic Circumpolar Current (ACC). By assuming the self-similarity as a hypothesis, Krupitsky *et al.* (1996) developed an equivalent barotropic (EB) model of the ACC capable of describing the horizontal structure of the ACC. Compared to the multi-level-primitive-equation GCM, the EB model appeared substantially simpler and therefore useful in pilot process-oriented and sensitivity studies. In the present study dynamical and kinematical comparisons of the EB and FRAM outputs are given.

1. Introduction

Recent numerical models with high spatial resolution, such as Semtner and Chervin (1988, 1992), the Fine Resolution Antarctic Model (FRAM) (see The FRAM group, 1991; Webb *et al.,* 1991), the Parallel Ocean Program (POP) model (see Dukowicz and Smith, 1994) and the Ocean Circulation and Climate Advanced Model (OCCAM), appeared sufficiently successful in simulating the dynamics of the Antarctic Circumpolar Current (ACC) and the whole of the Southern Ocean. The multi-level primitive equation GCMs, however, are very expensive for use in process-oriented studies or sensitivity experiments. Therefore the formulation of a simple dynamical model, capable of correctly describing the large-scale properties of the ACC, appears to be useful.

The analysis of the FRAM results by Killworth (1992) revealed an extremely interesting property: the time-mean velocity field in the ACC is close to being self-similar in the vertical, with the corresponding correlations between the velocity vectors at different depths exceeding 0.5 for most depths. By the vertical self-similarity we mean that the horizontal velocity vectors at different depths of a chosen vertical are colinear and

1. Department of Oceanography, University of Southampton, Southampton, United Kingdom, S014 3ZH.
2. Present address: Jet Propulsion Laboratory, California Institute of Technology, Pasadena, California, 91109, U.S.A. ***email: voi@sundog.jpl.nasa.gov***
3. Woods Hole Oceanographic Institution, Woods Hole, Massachusetts, 02543, U.S.A.
4. Department of Marine Science, The University of Southern Mississippi, Stennis Space Center, Mississippi, 39529 U.S.A.

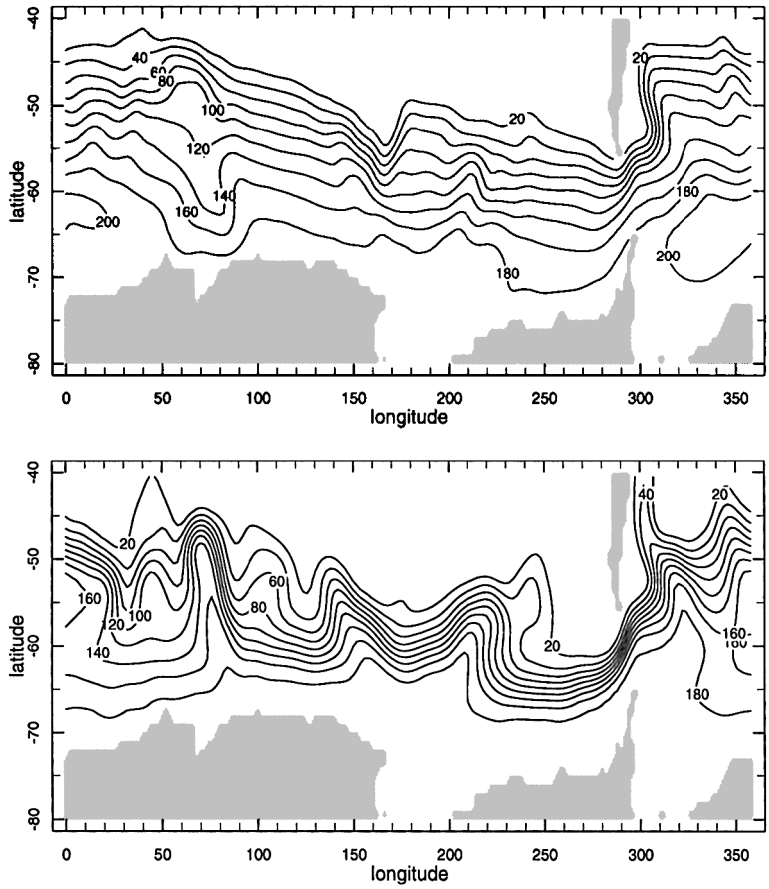

Figure 1. Isolines of the transport streamfunction. The units are in Sv. (a) for FRAM. The total transport across Drake Passage is 185 Sv. (b) for the EB model. The total transport is 182 Sv ($\varepsilon = 0.003$ m s^{-1}).

proportional to each other, with the coefficient of proportionality independent of the horizontal position.

Motivated by this observation, Krupitsky *et al.* (1996) developed a linear equivalent barotropic (EB) model where the self-similar vertical structure of the velocity field was prescribed. They derived a potential vorticity equation which appeared similar to the usual barotropic potential vorticity equation but with a modified expression for the ambient potential vorticity f/F, $F = \int_{-H}^{0} P(z)\, dz$, where $P(z)$ is the prescribed function describing the vertical structure of the ACC, and f is the Coriolis parameter.

The numerical experiments outlined in Krupitsky *et al.* (1996) showed that the transport streamfunction patterns calculated by the EB and FRAM models are qualitatively similar (see Figs. 1a,b).

In this paper we extend the comparison between the EB and FRAM models by analyzing in more detail the structure of the corresponding ACC transport streamfunctions. The comparison of zonally averaged momentum and vorticity balances in the EB and FRAM models will allow us to assess more completely the applicability of the EB model to the dynamical study of the ACC.

2. The numerical models

a. The Fine Resolution Antarctic Model (FRAM)

FRAM is a British numerical model of the Southern Ocean based on the GFDL approximations for the system of basic equations. It has a horizontal grid spacing of 0.25° in latitude, 0.5° in longitude and 32 depth levels. This corresponds to an average horizontal resolution of about 27 km at 60S, and a vertical resolution ranging from 20 m in the surface layer to 230 m in the bottom layer. FRAM uses the traditional formulation of the barotropic mode equation, which requires smoothing of the bottom topography to increase the numerical stability of the model (The FRAM Group, 1991) (see Fig. 2a).

The model domain covers an area from 24S to the Antarctica coastline. At the northern boundary an open boundary condition was used (Stevens, 1990).

The model was spun-up over six years using Levitus (1982) temperature and salinity climatology and Hellerman and Rosenstein (1983) wind stress. The integration was continued for a further ten years, with the final six years as an analysis phase. We apply the term "time mean" for the time average over the last six years of the integration. Further details of the model and its results can be found in the article by The FRAM Group (1991).

b. The Equivalent-Barotropic Model (EB)

The basic equations of the EB model are the steady state depth-averaged equations for zonal and meridional components of momentum and the depth-averaged continuity equation. The momentum equations balance the Coriolis force, the horizontal pressure gradient and the vertical turbulent friction; the nonlinear terms and the horizontal friction are neglected (Krupitsky *et al.,* 1996). Following the self-similarity hypothesis the horizontal pressure gradient, $\nabla_H p'$, is represented as $\nabla_H p' = P(z)\nabla_H p_s$ where $p' = p/\rho_0$, p is the pressure, ρ_0 is the mean density; $p_s = p_s(x, y)$ is the surface pressure; $P(z)$ is the prescribed vertical profile function; and ∇_H is the horizontal gradient operator.

The governing parameters of the model are the vertical profile function $P(z)$ and the bottom friction coefficient ε. In the simulation analyzed in this note we will use $P(z) = c_\infty + e^{z/H_0}$, where $c_\infty = 0.05$, $H_0 = 900$ m; and $\varepsilon = 3 \cdot 10^{-3}$ m s^{-1}. With such parameters the transport through the Drake Passage was found to be 182 Sv.

The depth-averaged potential vorticity equation for the model is as follows:

$$\varepsilon\left(\frac{\partial}{\partial x}\frac{P(-H)}{F^2}\frac{\partial \Psi}{\partial x} + \frac{\partial}{\partial y}\frac{P(-H)}{F^2}\frac{\partial \Psi}{\partial y}\right) + J\left(\Psi, \frac{f}{F}\right) = \mathrm{curl}_z\left(\frac{\tau}{F}\right) \qquad (1)$$

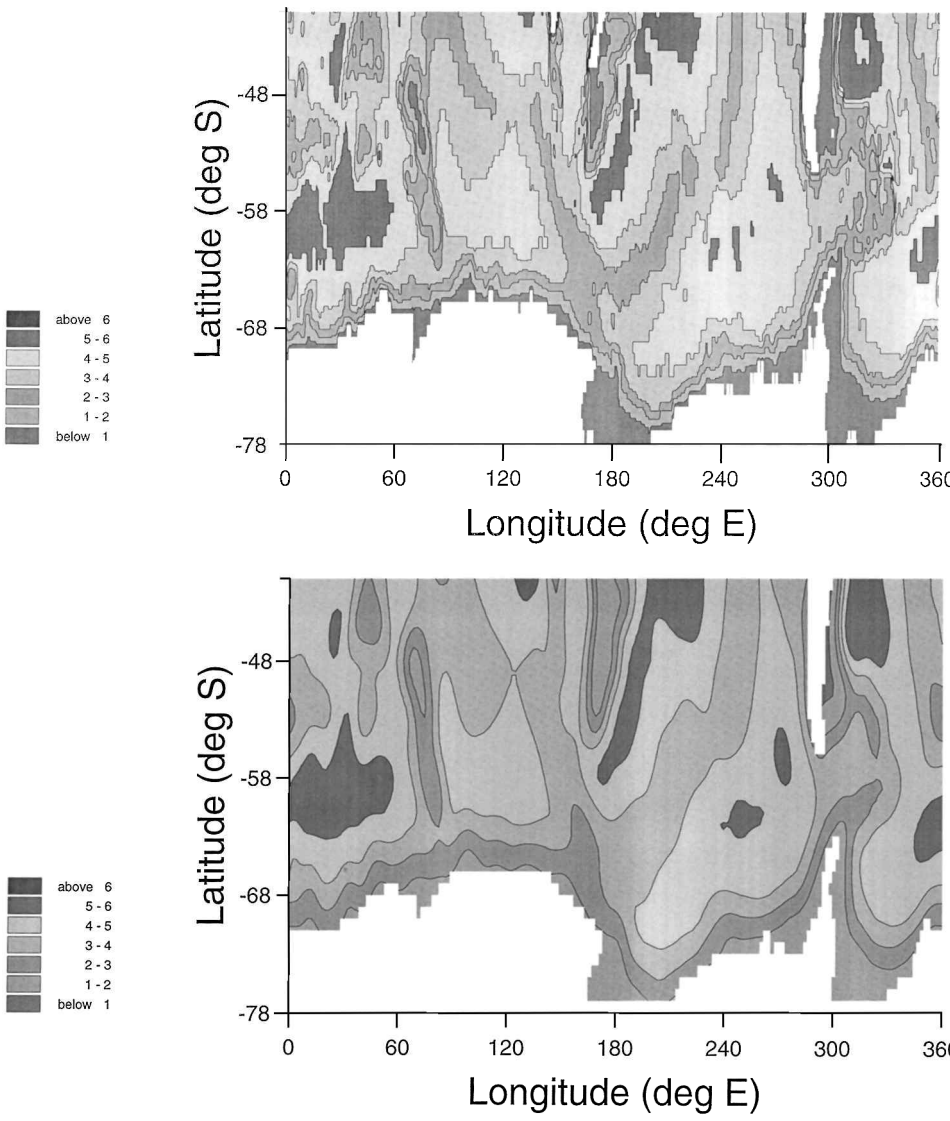

Figure 2. The bottom topography of the Southern Ocean in km (a) for FRAM. (b) for the EB model.

where Ψ is the transport streamfunction: $U = -\partial\Psi/\partial y$; $V = \partial\Psi/\partial x$; $(U, V) = \int_{-H}^{0} (u, v)\, dz$; u, v are the horizontal components of velocity; ε is a constant bottom friction coefficient; $F = \int_{-H}^{0} P(z)\, dz$; τ is the wind stress; $J(\Psi, f/F)$ is the Jacobian operator; the x-axis is directed to the east, and the y-axis is directed to the north.

The domain of integration is double-connected: the boundary consists of the southern boundary (the coastline of Antarctica), Γ_S, and the northern boundary (the latitude 40S and

the coastline of the South American continent), Γ_N. The boundary conditions are:

$$\Psi = 0 \text{ at } \Gamma_S; \qquad \Psi = T \text{ at } \Gamma_N. \tag{2}$$

The constant T is the total transport of the ACC to be determined from the condition:

$$\oint_\Gamma \left(\frac{f}{F} \frac{\partial \Psi}{\partial S} + \varepsilon \frac{P(-H)}{F^2} \frac{\partial \Psi}{\partial n} + \frac{\tau^s}{F} \right) ds = 0. \tag{3}$$

Here Γ is an arbitrary closed contour which lies within the domain of integration and embraces the Antarctic continent (Kamenkovich, 1961); **s** is the direction along Γ in a counter clockwise sense; **n** is orthogonal to Γ in such a way that (**s**, **n**, **k**) constitute the right-handed triplet, where **k** is the vertical unit vector; τ^s is the s-component of the wind stress.

The geography of the region was simplified to the maximum whereby all land masses except for S. America and Antarctica were submerged to 100 m. This simplification worked well, since even after smoothing the results of calculations, we did not observe any substantial currents across the areas where land was submerged.

The grid spacing is 0.2° in the zonal direction (x) and 0.1° in the meridional direction (y). The bottom topography was prepared by smoothly interpolating the ETOPO5 database on to a 0.2° × 0.1° grid (Krupitsky *et al.,* 1996), (see Fig. 2b). The steady-state wind stress was taken from Hellerman and Rosenstein (1983).

The sensitivity of the EB model to the parameters is studied in detail in Krupitsky *et al.* (1996; see Table 2). A very fine grid resolution is required for the numerical model to reproduce the theoretically predicted asymptotic behavior $T \sim \varepsilon^{-1}$ in the limit of very small friction coefficient ε. For finite values of the friction coefficient ε used in the calculations, the dependency is closer to $T \sim \varepsilon^{-1/2}$ and only a moderate resolution is required.

Note, that the EB model allows substantial computational savings; our estimation shows that this model is about 3 order of magnitudes quicker than a traditional primitive equation model, like the FRAM.

3. The dynamical balances

In this section we compare the time-mean, depth-integrated, and zonally-averaged terms in the FRAM momentum and vorticity equations with the corresponding zonally-averaged terms in the EB model. The zonal averaging applies in the zonally unbounded region of the Southern Ocean, that is on the Drake Passage latitudes (between 55.5S and 63.8S).

Stevens and Ivchenko (1997) showed that averaging the FRAM zonal momentum equation (over time, depth, and a latitude circle) gives to leading order the balance between the wind stress $\overline{[\tau_\lambda]}$ and the bottom pressure drag BPD,

$$\text{BPD} = \overline{\left[\frac{1}{a \cos \phi} \left(H \frac{\partial p_s}{\partial \lambda} + \int_{-H}^{0} \int_{z}^{0} g \frac{\partial \rho}{\partial \lambda} dz' dz \right) \right]}. \tag{4}$$

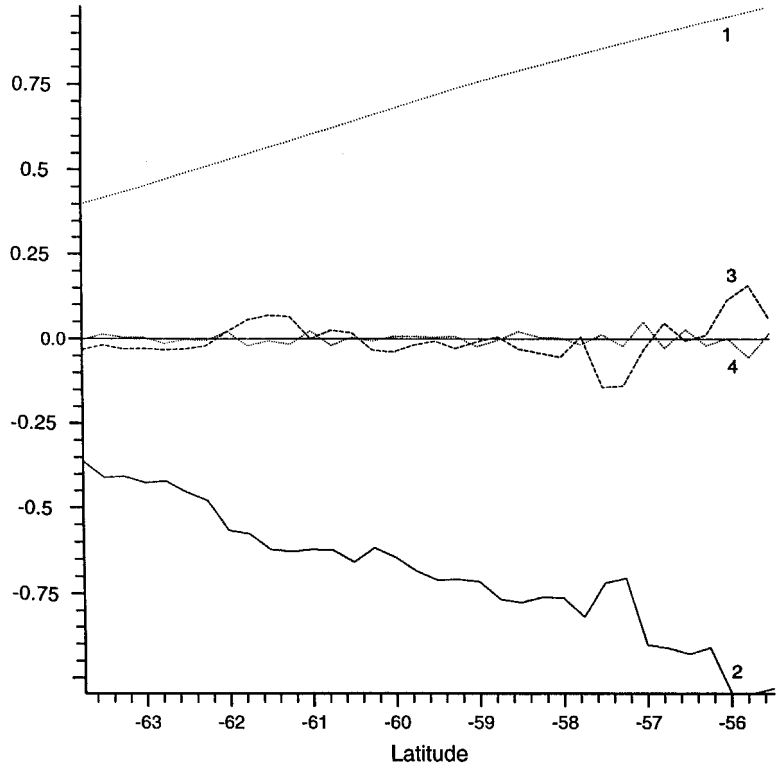

Figure 3. (a) The depth-integrated, time-mean, and zonally averaged terms in the FRAM zonal momentum equation as functions of the latitude. Lines 1, 2, 3 and 4 represent the zonal wind stress, bottom form drag, poleward momentum-flux divergence (that is $[(1/\alpha \cos\phi)(\partial/\partial\phi) \int_{-H}^{0} uv \cos\phi \, dz]$), and the sum of the remaining terms respectively (by Stevens and Ivchenko, 1997). (b) the same for the EB model. Lines 1, 2, and 3 represent the zonal wind stress, bottom form drag, and the bottom friction respectively. The units are in 10^{-4} m^2 s^{-2}.

The square bracket represents a zonal average and the overbar denotes a time average. The variables p_s, τ^{λ} and ρ refer to surface pressure, zonal wind stress and density, respectively. The radius of the Earth is a, the depth is H, g is the acceleration due to gravity; ϕ and λ are the latitude and longitude, respectively (Fig. 3a).

We obtain essentially the same balance for the EB model (Fig. 3b) (BPD is calculated as the difference between the zonally averaged bottom friction and the wind stress). The bottom friction appears relatively small and due to the zonal averaging the influence of the Coriolis acceleration is absent. It is worth stressing that the time-mean, depth-integrated, and zonally-averaged nonlinear terms and lateral friction in the momentum equations are negligible in FRAM (Stevens and Ivchenko, 1997). This is probably the main reason why the EB model, which contains neither nonlinear terms nor lateral friction, describes satisfactorily the depth-averaged velocity field (the transport field) of the ACC. This result

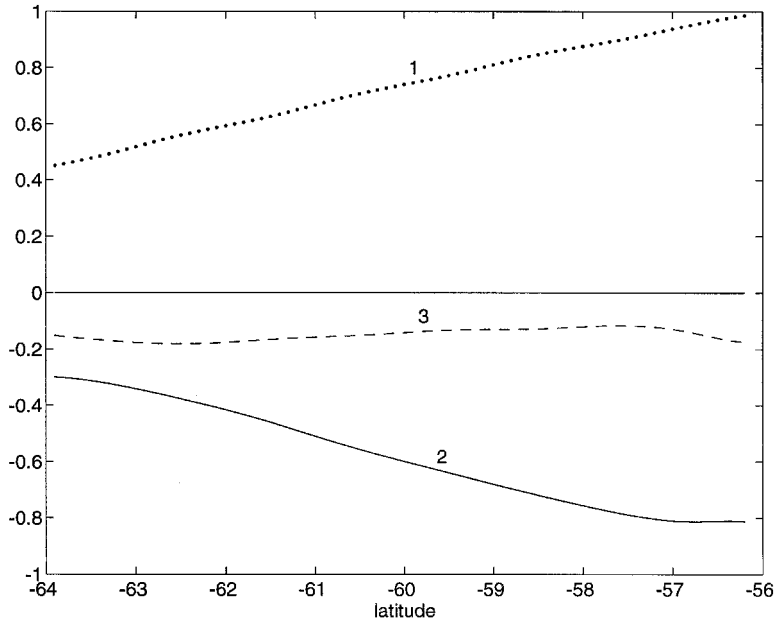

Figure 3. (Continued)

can be further illustrated by calculating zonally averaged streamfunctions in the two models (Fig. 4). The small misfit between the two curves shown in Figure 4 could be further decreased by tuning the bottom friction coefficient ε in the EB model.

It is worth noting that for the nearly geostrophic flows, regional balances of vertically averaged momentum equations are certain to be dominated by integrals of pressure gradient and the Coriolis terms. Zonal averaging removes these highest order terms and allows us to highlight the relationships between locally small (compared to pressure gradient and Coriolis term) but dynamically significant quantities that are otherwise overshadowed by the geostrophic terms. Additional calculations confirmed that the flows in both FRAM and EB models are close to geostrophic. So, for the EB model the rms values (over the whole domain) of the depth-averaged Coriolis acceleration and pressure gradients are approximately equal to each other. The rms values of the wind stress and bottom friction terms are two to three orders of magnitude smaller than those of the geostrophic terms (see Eqs. (4) and (5) in Krupitsky *et al.,* 1996).

Let us now turn to the vorticity equation. In FRAM, the depth-integrated vorticity equation is obtained (see Appendix) by the depth integration of the momentum equations and by taking the curl of these equations. The vorticity budget calculated is consistent with the FRAM model, so that the sum of the individual terms is equal to the time rate of the depth-integrated vorticity, to an accuracy of $<0.01\%$ of the leading terms. After time averaging the steady state balance holds to an accuracy of $<2\%$ of the leading terms (see

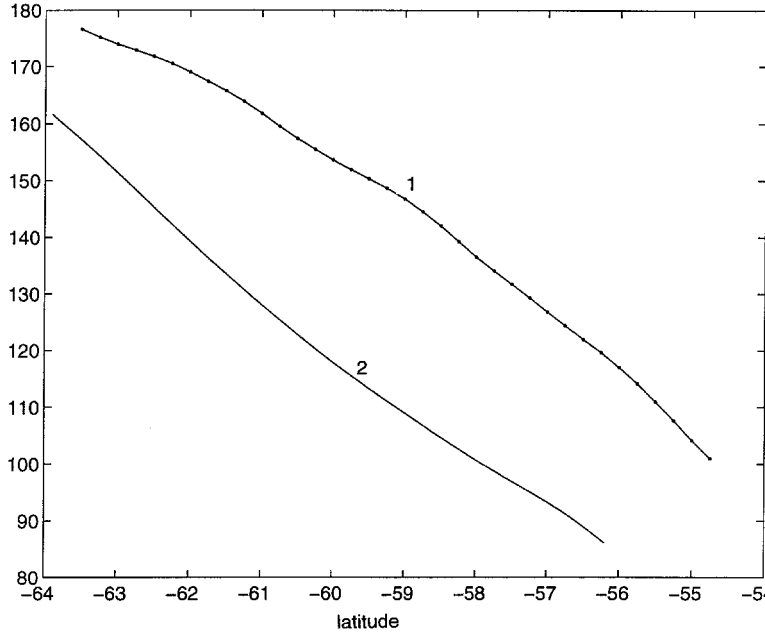

Figure 4. The time-mean and zonally-averaged transport streamfunction versus latitude (in Sverdrups). 1 and 2 refer to FRAM and the EB ($\varepsilon = 0.003$ m s^{-1}), respectively.

Table 1). The vorticity equation for the EB model is derived analogously by taking the curl of the depth integrated momentum equations of the model.

Figure 5a shows the individual terms in the FRAM vorticity budget (see notations in the Appendix). The individual terms show considerable variability between latitudes, despite the averaging along each circumpolar latitude circle (720 grid points). Though the wind stress curl is clearly seen, the bottom pressure torque, advection and lateral friction terms exhibit large changes with latitude. The FRAM vorticity budget is more complicated than the EB vorticity budget, because of the contribution from nonlinear advection and lateral friction terms which are not explicitly included in the EB model.

Table 1. The time-mean, zonally- and depth-averaged terms ($\times 10^{-12}$) in the FRAM vorticity equation for the latitude band from 55S to 63S (in m s^{-2}). See Appendix for notations.

WIND CURL	−79.1984
BOTTOM FRICTION	1.2404
BPT	+78.5122
LATERAL FRICTION	2.9093
ADVECTION	−4.8102
BETA	0.0
LHS	−1.3361
RHS	−1.3467

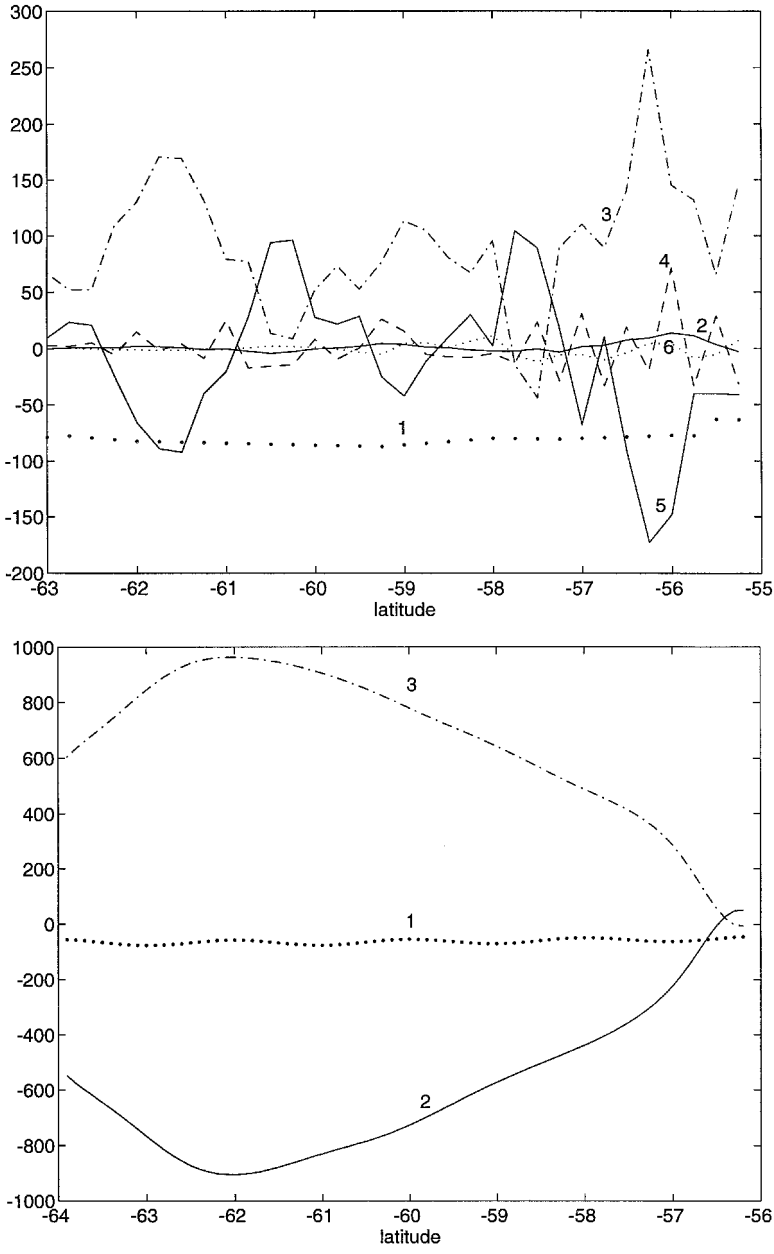

Figure 5. (a) The depth-integrated, time-mean, and zonally averaged terms in the FRAM vorticity equation as functions of the latitude. Lines 1, 2, 3, 4, 5 and 6 represent the wind stress curl, bottom friction, bottom pressure torque, lateral friction, advection and the sum of the previous five terms respectively (for notations see Appendix). (b) the same for the EB model. Lines 1, 2, 3 represent the wind stress curl, bottom friction, bottom pressure torque respectively. The units are 10^{-12} m s^{-2}.

Let us consider the advection at each latitude, and describe why it is significant. By summing the terms along a latitude circle from 0° eastward, it is found that the largest contribution is at 55S, at 150E and 150W longitudes. These two areas correspond to very strong gradients in the streamfunction between 70 and 120 Sv isolines, in the central core of the ACC. (See Fig. 1 from Wells and deCuevas, 1995.)

The other latitudes where advection is of major significance are at 60S and to a lesser extent, at 63S. At 60S the major contribution occurs at 70W–40W longitude, in the Drake Passage/Scotia Sea, whilst at 63S there is a sizeable contribution at 150W longitude.

Thus, there is no one subregion (e.g., Drake Passage) of the ACC, where all the advection is located.

The vorticity balance changes from one latitude to another due to local intensification of ACC around topographic obstacles. The tendency for a negative correlation between BPT and ADVECTION, gives some credence to the role of topography. In the EB model, because of the smoothing of the topography and the neglect of the nonlinear terms, strong local features cannot be produced.

When a summation is made over the whole band (Table 1), the leading order terms are BPT and WIND CURL, and the remaining terms are much smaller. For example, the ADVECTION is 6% of the BPT term. This is consistent with the averaged zonal momentum budget in FRAM, where the leading order balance is between the zonal wind stress and the bottom form drag (Stevens and Ivchenko, 1997).

The EB vorticity equation, when averaged over the circumpolar belt shows a substantially different budget to that of FRAM (see Fig. 5b). In EB the BPT is larger by a factor of 3 to 4, than in FRAM, with a single maximum at 62S. (In FRAM in addition to the maximum at 62S, there is a second maximum at 56S.) The BPT is balanced by the bottom friction in EB, with the wind stress curl being of second order. The large values of BPT can be explained by the greater role of the bottom friction in the EB model vorticity balance (as compared to the role of bottom friction in the corresponding FRAM balance). Note that the bottom friction is clearly very small in the zonally-averaged momentum budget of both FRAM and EB models.

4. The comparison of transport streamfunctions

In this section we will compare in detail the EB and FRAM transport streamfunctions. The FRAM field was smoothed by applying the method used in Krupitsky *et al.* (1996) and then interpolated into the grid 2° (in longitude) by 1° (in latitude) for the domain from 78.5S to 41.5 S. The EB solution was interpolated onto the same $2° \times 1°$ grid.

In Figure 6 a scatter-plot of FRAM vs. EB is shown where all the points from the domain are represented. There are two straight lines on that figure and on all the following scatter-plot figures. The first one (dashed line) is the linear regression of the y axis (i.e. FRAM) on the x axis (i.e., EB), and the second one (dashed-dotted line) is the reverse (see Table 2). The closer the two lines, the better is the correlation. The mean square deviation

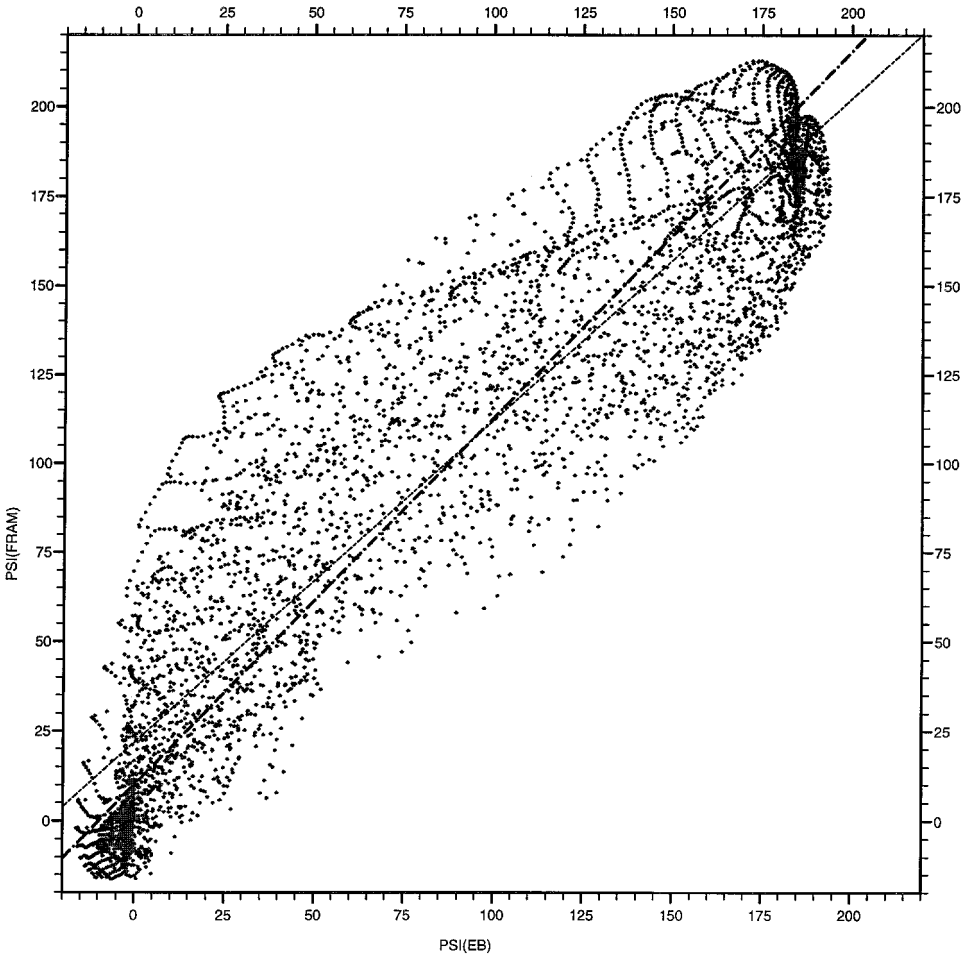

Figure 6. Scatter plot of the transport streamfunctions (FRAM vs. EB) using all of the points from 78.5S to 41.5S. The values are in Sv. The dashed line shows the linear regression of the *y* axis on the *x* axis, and the dash-dotted line is the reverse.

(MSD) about the regression of FRAM on EB is 648 Sv^2 and the coefficient of correlation $r = 0.94$.

Firstly we shall exclude the non-ACC points from the domain, that is all the points where the FRAM streamfunction is higher than 180 Sv or less than 10 Sv. We do not show the corresponding figure here because this case appears quite similar to the general case (Fig. 6) with the top and lowest points cut off. The correlation r is quite high, though it is smaller than in the previous case ($r = 0.87$); MSD = 642 Sv^2.

Secondly there is a good linear relationship between the zonally-averaged values of the FRAM and EB (see Fig. 7). The angle between the two lines of linear regression is very

Table 2. Mean values of the streamfunction over the whole domain $\{\overline{\Psi}\}$ (in Sv); the mean square of deviations (MSD) from the corresponding regression lines FRAM on EB (F/E) (in Sv^2); the coefficient of correlation (r) between FRAM and EB streamfunction; and the equation of the corresponding linear regression (F/E and E/F).

	$\{\overline{\Psi}\}$ (EB)	$\{\overline{\Psi}\}$ (FRAM)	MSD	r	Linear regression F/E	Linear regression E/F
Fig. 6	94.6	107.3	648.4	0.94	Ψ (FRAM) = 21.93 + 0.90 · Ψ (EB)	Ψ (FRAM) = 10.13 + 1.03 · Ψ (EB)
Fig. 8	105.0	115.7	76.0	0.99	Ψ (FRAM) = 13.21 + 0.98 · Ψ (EB)	Ψ (FRAM) = 11.65 + 0.99 · Ψ (EB)
Fig. 9	82.7	82.7	124.8	0.99	Ψ (FRAM) = 4.38 + 0.95 · Ψ (EB)	Ψ (FRAM) = 2.62 + 0.97 · Ψ (EB)
Fig. 10	61.9	80.3	1051.0	0.89	Ψ (FRAM) = 23.57 + 0.92 · Ψ (EB)	Ψ (FRAM) = 9.30 + 1.14 · Ψ (EB)

small, the correlation r is very high ($r = 0.99$) and MSD has 76 Sv^2, the lowest value among all calculated MSD (see Table 2).

In addition to this general comparison, a regional analysis has been made. The domain was separated into 18 subregions in longitude (0°–20E, 20E–40E, etc), and the scatter-plots of the EB and FRAM streamfunctions obtained.

The mean square deviation (MSD) about the regression of FRAM on EB for these subregions ranges between 124 Sv^2 and 1054 Sv^2 (see Table 2). After the preliminary analysis we merged several neighboring regions and recalculated correlation and regression coefficients, and MSD for the larger domains. The lower values of MSD occurred in the areas with pronounced topographical features, like the Crozet-Kerguelen area (40E–80E) where MSD = 575 Sv^2, the area to the southeast of the Australia (Macquarie-Ridge Complex and near the Pacific-Antarctic Ridge, 140E–120W) where MSD = 370 Sv^2, and to the east from the Drake Passage (60W–0°) where MSD = 471 Sv^2.

It is worth noting that the EB model satisfactorily describes such features as the strong turn of the southern flank of the ACC when the flow crosses the Pacific-Antarctic Ridge (160W–140W) and a similar strong turn of the ACC on the Macquarie-Ridge Complex (140E–160E).

In other areas, with a more quiet topography, like in the eastern part of the Indian Sector of the Southern Ocean (80E–140E) and in the Southeast Pacific Basin (120W–80W), we see larger values of MSD equal to 792 Sv^2 and 995 Sv^2, respectively.

The two examples of scatter plots for the local 20° areas are shown in Figures 8 and 9. The former corresponds to the Macquarie-Ridge Complex and the latter corresponds to the Southeast Pacific Basin.

The comparison between FRAM and EB models for the Southeast Pacific Basin, between 120W and 100W, gives the worst result with MSD equal to 1051 Sv^2 (see Fig. 9 and Table 2). It is quite clear that the FRAM flow in this region is much broader than the EB

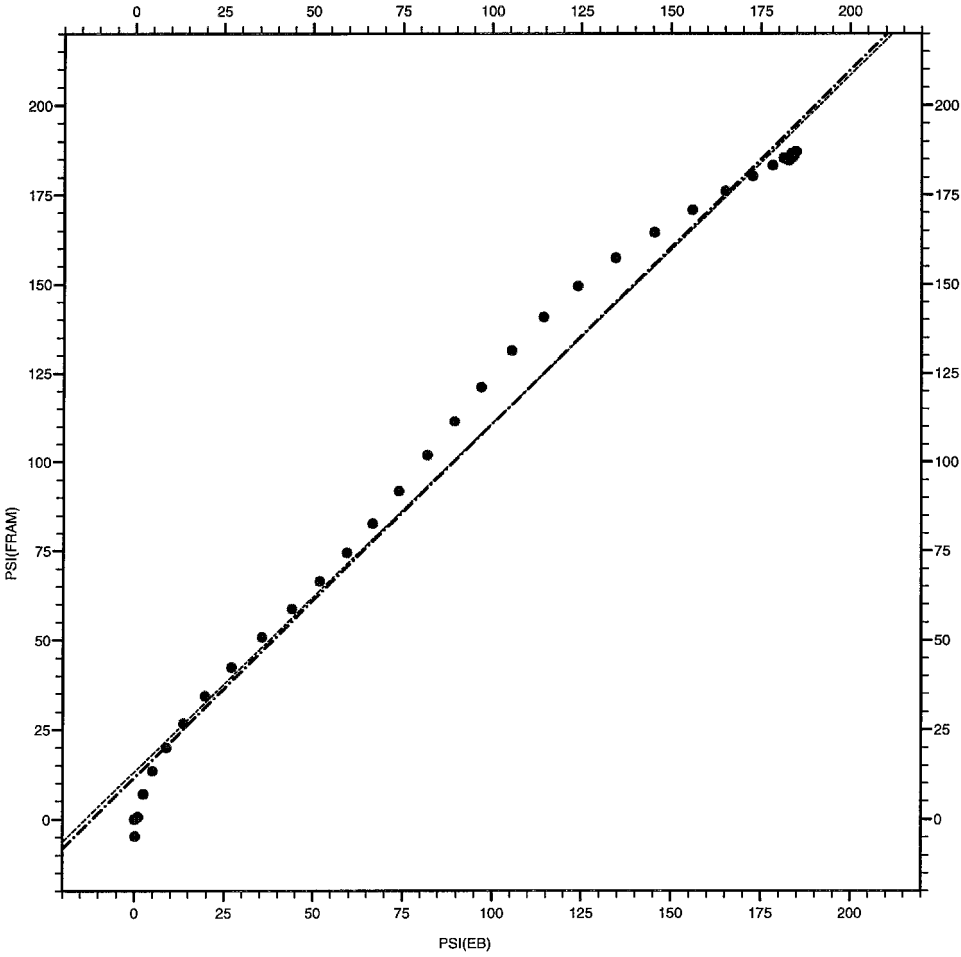

Figure 7. Scatter plot of the transport streamfunctions (FRAM vs. EB) for the zonally averaged streamfunctions. The regression lines are shown (see Table 2). The units are in Sv.

flow. One can infer from Figure 9 that different regressions lines are needed for the northern and southern flanks of the flow.

Thus, in those regions where the topographic features are well pronounced the agreement between the EB model and FRAM appeared satisfactory, whilst in the regions with less pronounced topography the agreement is worse. It seems that this is due to the different role of the bottom friction in both models in the regions with quiet bottom topography. The balance of terms in the EB model shows that the bottom friction appears more significant in the regions with less pronounced topography, as compared to the other regions: if the depth is almost constant, the flow will be very near to zonal, and the Jacobian term in (1) will be very small. In the FRAM model the bottom friction plays a negligible role everywhere.

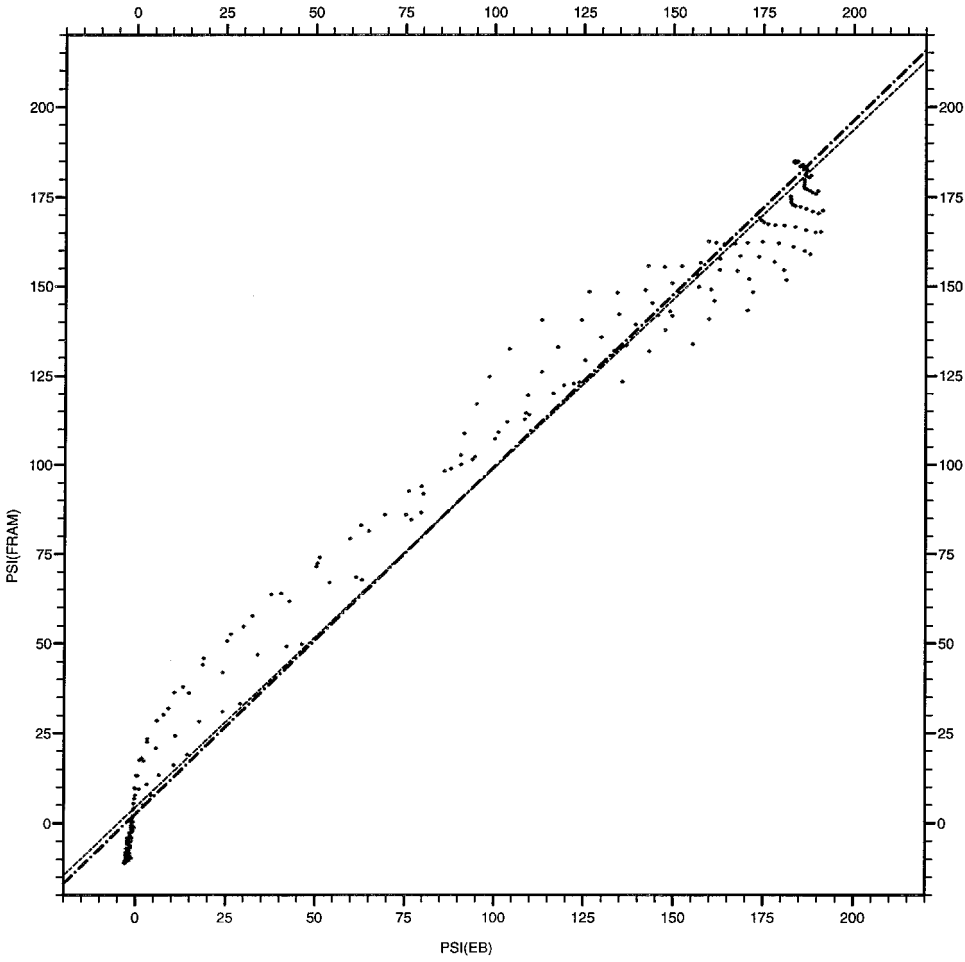

Figure 8. Scatter plot of the transport streamfunctions (FRAM vs. EB) for the subregion between 140E and 160E (Macquarie-Ridge Complex). The regression lines are shown (see Table 2). The units are in Sv.

5. Discussion and conclusions

The EB model was intended to describe the large-scale horizontal structure of the ACC. The simplicity of the model appeared very useful for some pilot process oriented and sensitivity studies (Krupitsky *et al.,* 1996). For example, it was shown that the dynamics of the ACC depends critically on whether the ambient-potential-vorticity f/F isolines ($F = \int_{-H}^{0} P(z)\, dz$, H is the depth) are closed or blocked in the region. This result highlights how the effect of bottom topography depends on the overall vertical stratification in the region. It was shown also that the wind stress itself is much more important than its curl (unlike the wind-driven circulation in a closed basin). The importance of this question was

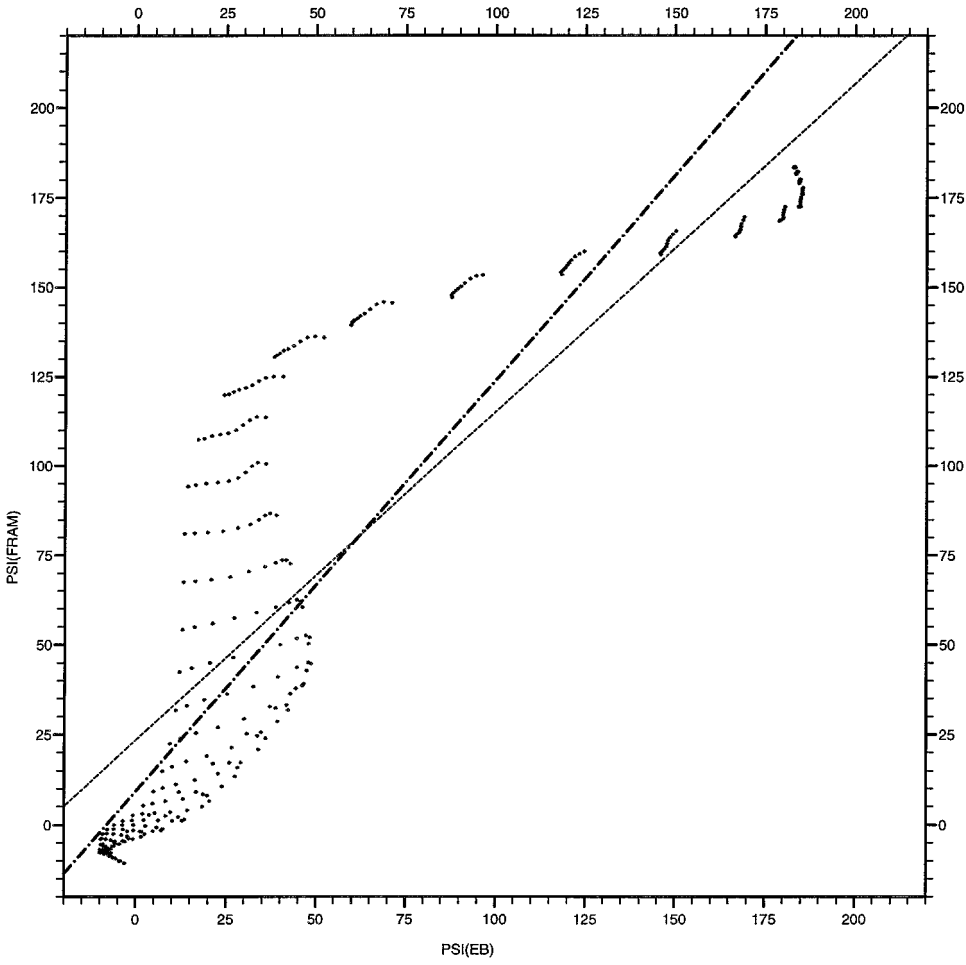

Figure 9. Scatter-plot of the transport streamfunctions (FRAM vs. EB) for the subregion in the Pacific Sector between 220E and 240E. The regression lines are shown (see Table 2). The units are in Sv.

confirmed in the recent discussion (see Olbers, 1998 and Warren *et al.,* 1996). Hopefully the EB model can be useful in some similar studies in the future.

It is worth noting also that some analytical methods can be applied to the EB model studies, due to its simplicity. The asymptotic analysis predicts the different role of friction in the "boundary" layers and in the "interior," which is helpful for regional analysis. Analytical results can help also in the development of an effective numerical model of the ACC.

To assess the applicability of the EB model to the analysis of the horizontal structure of the ACC, we performed a comparison of the EB model results with the time-mean depth-averaged results of the FRAM model. The horizontal structure of the ACC transport

streamfunction appears reasonably similar in both models (see Figs. 1 and 6). The more detailed regional analysis shows a rather satisfactory agreement in the regions with pronounced topographic features (Crozet-Kerguelen area, 20E–80E; Macquarie-Ridge Complex and near Pacific-Antarctic Ridge, 140E–120W; and to the east from the Drake Passage, 60W–0°). In the regions with a more quiet topography (eastern part of the Indian Sector of the Southern Ocean, 80E–140E; and in the Southeast Pacific Basin, 120W–80W) the agreement is worse. This seems to be due to the different role of the bottom friction in both models. In the FRAM the bottom friction is negligible everywhere, whilst in the EB model it appears to be more significant in the regions with the less pronounced bottom topography.

It is known (Stevens and Ivchenko, 1997) that the averaged (over time, depth and a latitude circle) FRAM zonal momentum equation provides the balance essentially between the wind stress and the bottom pressure drag. The same averaged momentum balance is given by the EB model.

The zonally averaged EB vorticity equation gives a substantially different budget to that of FRAM. The bottom pressure torque in the EB model is larger by a factor of 3 to 4 (as compared to FRAM) and is balanced by the bottom friction. In FRAM the corresponding averaged balance is essentially between the bottom pressure torque and the wind stress curl. It is probable that the EB model exaggerates the role of the bottom friction in the vorticity balance.

Acknowledgments. We gratefully acknowledge the help and support of the FRAM team in providing the data from the numerical model experiment. V. O. Ivchenko was supported by the NERC under grant GST/02/0817 and by an NRC Resident Research Associateship (NASA Code Y).

APPENDIX

The vorticity budget in FRAM

The depth-integrated vorticity budget is derived taking the curl of the depth-integrated momentum equations. The resulting equation is:

$$\frac{\partial}{\partial t}\nabla^2\Psi = k\cdot\nabla\times\left(f\nabla\Psi + \tau - \int_{-H}^{0}\nabla p dz + \mathbf{F} + \mathbf{N} - \tau_{\mathbf{b}}\right) \tag{A1}$$

where Ψ is the streamfunction, p is the pressure, $\mathbf{F}$ is the vertical integral of the lateral friction terms, $\mathbf{N}$ is the vertical integral of the nonlinear advection terms, $\tau_{\mathbf{b}}$ is the bottom stress, $\mathbf{k}$ is the unit vertical vector.

Eq. (A1) may be rewritten:

$$\frac{\partial}{\partial t}\nabla^2\Psi = \mathbf{k}\cdot\nabla\times(\tau - \tau_{\mathbf{b}}) - J[p_b, H] + \mathbf{k}\cdot\nabla\times(\mathbf{F} + \mathbf{N} + f\nabla\Psi) \tag{A2}$$

where p_b is the bottom pressure.

Since the pressure in the model is given by the hydrostatic relation, we have

$$J[p_b, H] = J[p_s, H] = J\left[\int_{-H}^{0} g\nabla\rho \, dz, H\right]. \tag{A3}$$

The terms on the right-hand side of (A2) will be referred to as WIND CURL, BOTTOM FRICTION, BPT, LATERAL FRICTION, ADVECTION, and BETA in order that appear in (A2).

REFERENCES

Dukowicz, J. K. and R. D. Smith. 1994. Implicit free-surface method for the Bryan-Cox-Semtner ocean model. J. Geophys. Res., *99,* 7991–8014.

Hellerman, S. and M. Rosenstein. 1983. Normal monthly wind stress over the World Ocean with error estimates. J. Phys. Oceanogr., *13,* 1093–1104.

Kamenkovich, V. M. 1961. The integration of the marine current theory equations in multiply connected regions. Doklady of the Academy of Sciences of the USSR, Earth Sciences Section, *138,* 629–631 (Translated from Russian).

Killworth, P. D. 1992. An equivalent-barotropic mode in the Fine Resolution Antarctic Model. J. Phys. Oceanogr., *22,* 1379–1387.

Krupitsky, A., V. M. Kamenkovich, N. Naik and M. A. Cane. 1996. A linear equivalent barotropic model of the Antarctic Circumpolar Current with realistic coastline and bottom topography. J. Phys. Oceanogr., *26,* 1803–1824.

Levitus, S. 1982. Climatological Atlas of the World Ocean. NOAA Prof. Pap., *13,* U.S. Dept. of Commerce, 173 pp.

Olbers, D. 1998. Comments on "On the obscurantist physics of 'form drag' in theorizing about the Circumpolar Current." J. Phys. Oceanogr., *28,* 1647–1654.

Semtner, A. J. and R. M. Chervin. 1988. A simulation of the Global Ocean circulation with resolved eddies. J. Geophys. Res., *93,* 15502–15522.

—— 1992. Ocean general circulation from a global eddy-resolving model. J. Geophys. Res., *97,* 5493–5550.

Stevens, D. P. 1990. On open boundary conditions for three dimensional primitive equation ocean circulation models. Geophys. Astrophys. Fluid Dyn, *51,* 103–133.

Stevens, D. P. and V. O. Ivchenko. 1997. The zonal momentum balance in an eddy-resolving general-circulationmodel of the Southern Ocean. Quart. J. Roy. Meteor. Soc., *123,* 929–951.

The FRAM group. 1991. Initial results from a fine resolution model of the Southern Ocean. EOS, Trans. Amer. Geophys. Union, *72,* 174–175.

Warren, B. A., J. H. LaCasce and P. E. Robbins. 1996. On the obscurantist physics of 'form drag' in theorizing about the Circumpolar Current. J. Phys. Oceanogr., *26,* 2297–2301.

Webb, D. J., P. D. Killworth, A. C. Coward and S. R. Thompson. 1991. The FRAM Atlas of the Southern Ocean. Natural Environment Research Council, Swindon, U.K., 67 pp.

Wells, N. C. and B. A. deCuevas. 1995. Depth integrated vorticity budget of the Southern Ocean from a general circulation model. J. Phys. Oceanogr., *25,* 2569–2582.

Received: *4 May, 1998;* revised: *6 October, 1998.*